Journal of **RAMAN SPECTROSCOPY**

Hyper-Raman and Raman scattering in paratellurite TeO$_2$

Vincent Rodriguez,[a]* Michel Couzi,[a] Frédéric Adamietz,[a] Marc Dussauze,[a] Guillaume Guery,[a,b,c] Thierry Cardinal,[b] Philippe Veber,[b] Kathleen Richardson[c] and Philippe Thomas[d]

Raman spectra of the tetragonal D_4^4 structure of paratellurite TeO$_2$ have been revisited avoiding anomalous polarization-selection-rules violations previously observed and due to optical activity. We present a complementary hyper-Raman scattering study of paratellurite. Wavenumber and symmetry assignments are given for all expected 21 Raman active optical branches, except one LO component (out of the eight expected TO–LO pairs) of the polar doublet E modes. Also, the four expected hyper-Raman active A$_2$ (TO) modes have been observed. Moreover, we have observed a strong Kleinman-disallowed hyper-Rayleigh signal, which is tentatively assigned as a first evidence of hyper-Rayleigh optical activity. Copyright © 2013 John Wiley & Sons, Ltd.

Keywords: hyper-Raman; hyper-Rayleigh; phonon; TO–LO modes; paratellurite

Introduction

The natural tellurium dioxide (tellurite TeO$_2$) is found as a metastable polymorph known as β-TeO$_2$, with space group Pbca (D_{2h}^{15}).[1] This phase transforms irreversibly at 600 °C to the stable polymorph under normal temperature and pressure conditions, known as paratellurite (α-TeO$_2$) with space group P4$_1$2$_1$2 (D_4^4).[2] Under hydrostatic pressure, α-TeO$_2$ undergoes a continuous (second order) phase transition at about 9 kbar to an orthorhombic phase with space group P2$_1$2$_1$2$_1$ (D_2^4).[3] This is up to now a unique example of 'pure' ferroelastic phase transition, which is not driven by any optical or relaxational soft mode.[4] More recently, two other metastable phases (the γ and δ phases) were evidenced by crystallization of TeO$_2$-based glasses. The γ phase belongs to the P2$_1$2$_1$2$_1$ (D_2^4) space group with no simple relation with the high-pressure phase of paratellurite, and a 'statistical' fluorite-like structure with Fm$\bar{3}$m (O_h^5) space group was proposed for the disordered ('antiglass') δ phase.[5,6]

The paratellurite structure that belongs to the crystalline class D$_4$ lacks a center of inversion and is also potentially optically active.[7] The TeO$_2$ single crystals, grown by the Czochralski method using [110] oriented seed, are transparent in the whole visible–near-infrared (IR) range with high and strongly birefringent refractive indices; furthermore, their elastic constants result in an extremely slow [110] shear wave, at the origin of the high-pressure phase transition. These characteristics lead to interesting piezoelectric, acousto-optic, and nonlinear optical applications.[8–12] In addition, TeO$_2$ is a glass former, and the tellurite-based glasses are very promising materials because of their remarkable optical properties: For instance, their third-order nonlinear susceptibility ($\chi^{(3)}$) appears amongst the highest ones never obtained in oxide glasses (more than 40 times higher than silica-based glasses measured in a nonresonant regime). Also, these glasses become efficient frequency doublers after thermal poling.[13] IR spectroscopy and Raman scattering (RS) are widely used techniques to characterize the short-range and

medium-range structures of amorphous materials,[14] and in this context, the precise knowledge of the vibrational spectra of the related crystalline phases is a necessary prerequisite to model the structure and properties of the glassy state.

In the present case, only a few publications were concerned with IR and RS studies of α-TeO2 single crystals.[15–19] Some discrepancies existed between the different authors in the assignment of the observed vibrational modes. On the one hand, the interpretation of the IR data depended on the accuracy of the reflectivity measurements and also on the model of dielectric function adopted to fit the spectra. On the other hand, the Raman data were influenced by the strong optical activity of paratellurite[20] that perturbed in an uncontrolled manner the polarization properties of the incident and scattered lights, resulting in the observation of 'anomalous polarization-selection-rules violations'[17] that made insecure the interpretation of the spectra.

In this paper, the Raman spectra of paratellurite are revisited. We show that it is possible to get rid of the influence of the optical activity in the plane perpendicular to the fourfold axis and then to interpret correctly the remaining anomalous polarization-selection-rules violations due to the optical activity along

* Correspondence to: Vincent Rodriguez, Institut des Sciences Moléculaires – CNRS UMR 5255, Université de Bordeaux, 33405 Talence, France
E-mail: vincent.rodriguez@u-bordeaux1.fr

a Institut des Sciences Moléculaires – CNRS UMR 5255, Université de Bordeaux, 33405, Talence, France

b CNRS, Université de Bordeaux, ICMCB UPR 9048, 87 avenue du Dr A. Schweitzer, Pessac, F-33608, France

c School of Materials Science and Engineering, COMSET, Clemson University, Clemson, SC, 29634, USA
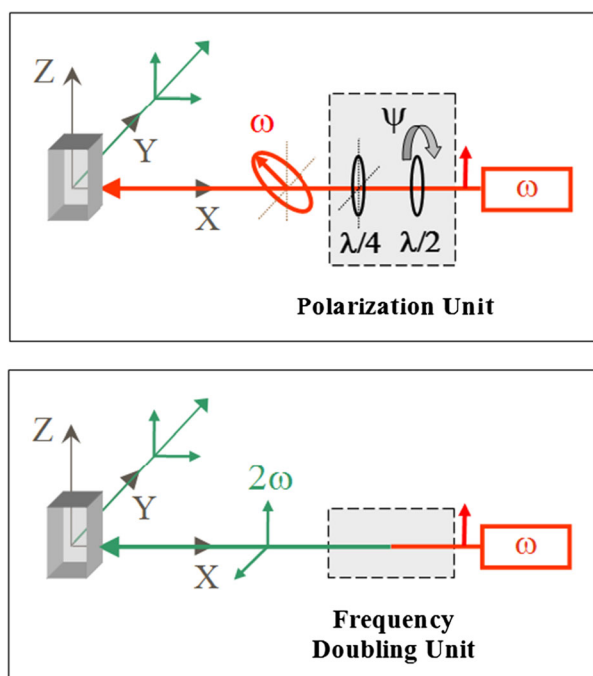
d Laboratoire Science des Procédés Céramiques et de Traitements de Surface, UMR 7315 CNRS, Centre Européen de la Céramique, 12 rue Atlantis, 87068, Limoges Cedex, France

the unique axis. Also, we present for the first time a study of the hyper-RS (HRS) spectra of paratellurite that complements the IR and RS data. These data will be used as reference for further works concerning the optical and spectroscopic properties of tellurite-based glasses.

Experimental setup for the collection of both Raman and hyper-Raman scattering

We consider spontaneous Raman and hyper-Raman/hyper-Rayleigh (also called harmonic light scattering or HLS) processes in transparent materials (far from any resonance). Therefore, RS and HRS responses that we consider involve only fully symmetric tensors of normal modes.[21] For that purpose, the experimental setup is configured in a classical 90° scattering geometry both for RS and HRS/HLS detection (Fig. 1), and it is based on a previous setup[22] that has been upgraded.[23] The incident radiation at 1064 nm is obtained from a passively mode-locked Nd:YVO$_4$ laser (EKSPLA) producing trains of 65 ps, ≤50 µJ pulses at a repetition rate of 2 kHz.

In the hyper-Raman/hyper-Rayleigh scheme (Fig. 1, top), we detect the scattered light at the optical frequency $2\omega - \omega_Q$ (Stokes response) from an intense incident laser pulsed at ω, where ω_Q denotes the frequency of a normal mode of vibration Q. Selection rules of spontaneous HRS have been widely discussed in the literature.[21,24–26] The HLS signal, i.e. the quasi-elastic/elastic part where $\omega_Q \to 0$, is indicative of the structure[27] (in terms of intensity) and of the dynamics[28,29] (in terms of width and profile) of the molecules or elementary structural units that constitute the crystal. The direction of the incident radiation is set along X, and a rotating half-wave plate controls the rotation of the plane of the incident polarization, giving thus a vertical (V), horizontal (H), or 45° incident polarization. When necessary,

the introduction of a fixed quarter-wave plate after the half-wave plate gives elliptical or circular states of polarization characterized by the angle ψ (Fig. 1, top). The polarized incident laser beam is then focused onto the sample using a 5× Mitutoyo Plan APO near-IR objective (infinity corrected with NA = 0.14) and positioned to pass at a distance of 1–2 mm from the inside of the crystal side facing the collecting lens. The incident laser beam waist had a diameter of ~10 µm with a Rayleigh range ~200 µm. The scattered light is collected at 90° in the Y direction; it is analyzed either vertically or horizontally by means of a polarizer and then focused with f/1.7 optics into a Horiba spectrograph as described elsewhere.[22] The entrance slits of the spectrograph were closed to fit the full beam waist image. The spectrally dispersed light (using a 1800 grooves/mm grating) was detected by a nitrogen cooled charge-coupled device camera (2048 × 512 pixels) in a continuous acquisition mode, with a spectral resolution better than 5 cm^{-1}. Incident radiation with energy less than 5 µJ has been applied because paratellurite is very sensitive to strong energy pulse as it triggers self-focusing (optical Kerr effect) into the crystal. Hence, hyper-Raman spectra were obtained with acquisition times of 120–240 s, depending on the scattering geometry, repeated four times to improve the signal-to-noise ratio. This setup has been successfully used for hyper-Raman and Raman studies of several liquids and solids.[23,30]

The scattering geometries are denoted by $X(IJK)Y$, using an extended Porto's notation.[25,31] Here, (J,K) and I denote the polarization directions of the biphotonic excitation and of the scattered light, respectively. Hence, the HV 90° scattering geometry will be noted $X(ZYY)Y$ (Fig. 1, top), thus probing the β_{ZYY} HRS tensor component.[25]

The Raman scheme (Fig. 1, bottom) is classical except that we use a pulsed source operating at 532 nm by frequency doubling the fundamental IR radiation using an NLO crystal in phase-matching condition. The fundamental beam at 1064 nm is rejected using a bandpass density filter. Hence, we detect the Raman scattered light at the optical frequency $2\omega - \omega_Q$ (Stokes response) from an incident laser pulsed at 2ω, where ω_Q again denotes the frequency of a normal mode of vibration Q. The scattering geometries are noted according to the classical Porto's notation.[31] Hence, the HV 90° RS geometry (Fig. 1, bottom) will be noted $X(YZ)Y$, thus probing the α_{YZ} Raman tensor component. Raman backscattering polarized experiments have also been performed using a micro-Raman spectrometer HR-800 from Horiba/Jobin-Yvon coupled with a continuous laser source emitting at 532 nm. For both Raman configurations, the spectral resolution was ~4 cm^{-1}, and Raman spectra were obtained with acquisition times less than 5 s in any case but repeated 15 times to improve the signal-to-noise ratio.

Symmetry properties of paratellurite

As mentioned already, the crystal of paratellurite (α-TeO$_2$) belongs to the P4$_1$2$_1$2 (D_4^4) space group. The primitive unit cell contains four formula units, with the tellurium atoms in positions 4(a) (x, x, 0), with C$_2$ site symmetry, and the oxygen atoms in general positions 8(b) (x, y, z),[2] resulting in 33 optical phonon branches with Γ-point symmetries 4A$_1$ + 4A$_2$ + 5B$_1$ + 4B$_2$ + 8E. The three acoustic modes of zero frequency at zone-center belong to A$_2$ + E symmetry. The singlet A$_2$ modes are IR active in the extraordinary ray spectrum, and the doublet E modes are IR active in the ordinary ray spectrum. The A$_1$, B$_1$, B$_2$, and E modes

Figure 1. Sketch of the experimental setup for hyper-Raman (top) and Raman (bottom) in the right angle scattering geometry.

are Raman active, whereas the A$_2$, B$_1$, B$_2$, and E modes are hyper-Raman active. Note that the A$_2$ and E polar modes exhibit TO–LO splitting in the close vicinity of the Brillouin zone center, which is probed by the IR, RS, and HRS techniques. For the D$_4$ point group, the Raman and hyper-Raman tensors of the different symmetry types in the Oxyz frame (where Ox is parallel to the [100] crystallographic direction, Oy is parallel to [010], and Oz is parallel to [001]) are of the form[21,24,25,32]

Raman:

$$A_1 : \begin{pmatrix} \alpha & 0 & 0 \\ 0 & \alpha & 0 \\ 0 & 0 & \beta \end{pmatrix}, \quad B_1 : \begin{pmatrix} \gamma & 0 & 0 \\ 0 & -\gamma & 0 \\ 0 & 0 & 0 \end{pmatrix}, \quad B_2 : \begin{pmatrix} 0 & \delta & 0 \\ \delta & 0 & 0 \\ 0 & 0 & 0 \end{pmatrix}$$

$$E_x : \begin{pmatrix} 0 & 0 & 0 \\ 0 & 0 & \varepsilon \\ 0 & \varepsilon & 0 \end{pmatrix}, E_y : \begin{pmatrix} 0 & 0 & -\varepsilon \\ 0 & 0 & 0 \\ -\varepsilon & 0 & 0 \end{pmatrix} \quad (1)$$

Hyper-Raman:

$$A_{2,z} : \begin{pmatrix} 0 & 0 & 0 & 0 & \beta & 0 \\ 0 & 0 & 0 & \beta & 0 & 0 \\ \beta & \beta & \alpha & 0 & 0 & 0 \end{pmatrix}, \quad B_1 : \begin{pmatrix} 0 & 0 & 0 & \gamma & 0 & 0 \\ 0 & 0 & 0 & 0 & \gamma & 0 \\ 0 & 0 & 0 & 0 & 0 & \gamma \end{pmatrix}$$

$$B_2 : \begin{pmatrix} 0 & 0 & 0 & 0 & \delta & 0 \\ 0 & 0 & 0 & -\delta & 0 & 0 \\ \delta & -\delta & 0 & 0 & 0 & 0 \end{pmatrix}$$

$$E_x : \begin{pmatrix} \varepsilon & \eta & \mu & 0 & 0 & 0 \\ 0 & 0 & 0 & 0 & 0 & \eta \\ 0 & 0 & 0 & 0 & \mu & 0 \end{pmatrix}, \quad E_y : \begin{pmatrix} 0 & 0 & 0 & 0 & 0 & \eta \\ \eta & \varepsilon & \mu & 0 & 0 & 0 \\ 0 & 0 & 0 & \mu & 0 & 0 \end{pmatrix} \quad (2)$$

As already pointed out, paratellurite exhibits strong optical activities along the three principal crystallographic directions that lead to the observation of strongly perturbed polarization-selection-rules in RS experiments.[17] Indeed, for crystals belonging to the class 422 (D$_4$), the nonzero components of the spontaneous gyration pseudo-tensor are $g_{11} = g_{22}$ (g) and g_{33} (g),[7,33] and according to Mamedov *et al.*,[20] the absolute value of g is twice as that of g, with g positive and g negative in α-TeO$_2$. The measured value of the rotatory power ρ along Oz (related to g_{33}) is around 29°/mm at 1064 nm and around 143°/mm at 532 nm. This strong dispersion of the rotatory power is concomitant with a strong dispersion of the refractive indexes in the visible range.[34,35]

In particular, the ordinary (n_o) and extraordinary (n_e) refractive indices measured at 532 nm are respectively 2.3001 and 2.4602, and those measured at 1064 nm are respectively 2.2005 and 2.3431.[12] To minimize the effect of the optical activity in the Oxy plane, we have prepared a crystal in the form of a parallelepiped (9.0 × 6.5 × 6 mm^3) with surfaces cut and polished perpendicular to the crystallographic [110], [1$\bar{1}$0], and [001] directions, respectively, checked by a Laue analysis. Indeed, it can be shown for the crystalline class D$_4$ that the [110] and [1$\bar{1}$0] directions are very less sensitive in the Oxy plane,[36,37] so that no effective optical activity is expected for incident or scattered light propagating in these directions. Under these conditions, we are just left with the optical activity occurring along [001] related to g_{33}. So, in the new O$x'y'z$ frame (Ox' is set parallel to [110], Oy' parallel to [1$\bar{1}$0], and Oz parallel to [001]), the Raman and hyper-Raman tensors become

Raman:

$$A_1 : \begin{pmatrix} \alpha & 0 & 0 \\ 0 & \alpha & 0 \\ 0 & 0 & \beta \end{pmatrix}, \quad B_1 : \begin{pmatrix} 0 & -\gamma & 0 \\ -\gamma & 0 & 0 \\ 0 & 0 & 0 \end{pmatrix}, \quad B_2 : \begin{pmatrix} \delta & 0 & 0 \\ 0 & -\delta & 0 \\ 0 & 0 & 0 \end{pmatrix}$$

$$E_x : \frac{1}{\sqrt{2}} \begin{pmatrix} 0 & 0 & \varepsilon \\ 0 & 0 & \varepsilon \\ \varepsilon & \varepsilon & 0 \end{pmatrix}, \quad E_y : \frac{1}{\sqrt{2}} \begin{pmatrix} 0 & 0 & -\varepsilon \\ 0 & 0 & \varepsilon \\ -\varepsilon & \varepsilon & 0 \end{pmatrix} \quad (3)$$

Hyper-Raman:

$$A_{2,z} : \begin{pmatrix} 0 & 0 & 0 & 0 & \beta & 0 \\ 0 & 0 & 0 & \beta & 0 & 0 \\ \beta & \beta & \alpha & 0 & 0 & 0 \end{pmatrix}, \quad B_1 : \begin{pmatrix} 0 & 0 & 0 & 0 & \gamma & 0 \\ 0 & 0 & 0 & -\gamma & 0 & 0 \\ \gamma & -\gamma & 0 & 0 & 0 & 0 \end{pmatrix}$$

$$B_2 : \begin{pmatrix} 0 & 0 & 0 & -\delta & 0 & 0 \\ 0 & 0 & 0 & 0 & -\delta & 0 \\ 0 & 0 & 0 & 0 & 0 & -\delta \end{pmatrix}$$

$$E_x : \frac{\sqrt{2}}{4} \begin{pmatrix} (\varepsilon + 3\eta) & (\varepsilon - \eta) & 2\mu & 0 & 0 & -(\varepsilon - \eta) \\ -(\varepsilon - \eta) & -(\varepsilon + 3\eta) & -2\mu & 0 & 0 & (\varepsilon - \eta) \\ 0 & 0 & 0 & -2\mu & 2\mu & 0 \end{pmatrix}$$

$$E_y : \frac{\sqrt{2}}{4} \begin{pmatrix} (\varepsilon + 3\eta) & (\varepsilon - \eta) & 2\mu & 0 & 0 & (\varepsilon - \eta) \\ (\varepsilon - \eta) & (\varepsilon + 3\eta) & 2\mu & 0 & 0 & (\varepsilon - \eta) \\ 0 & 0 & 0 & 2\mu & 2\mu & 0 \end{pmatrix} \quad (4)$$

The microscopic origin of the remarkable properties of paratellurite is still far for final clarity, but the authors generally agree that they are related to the peculiarities in the short-range atomic ordering around the tellurium atom. As shown in Fig. 2 (a), the tellurium atoms in paratellurite have four neighboring oxygen atoms so that the elementary structural unit is a TeO$_4$ disphenoid or, if we take into accounts the 5s^2 lone pair of tellurium atom (E), a distorted TeO$_4$E trigonal bipyramid unit. In this bipyramid, the two equatorial oxygen atoms O$_{eq}$ are separated from Te by distances (0.1878(1) nm) shorter than the sum of the covalent radii of O and Te atoms (0.208 nm) and the two axial oxygen atoms O$_{ax}$ by distances (0.2122(1) nm) longer than that value.[2] The α-TeO$_2$ paratellurite structure is built from such TeO$_4$ units sharing corners, as shown in Fig. 2(b). This results in the existence of highly asymmetrical Te–$_{eq}$O$_{ax}$–Te bridges involving one short Te–O$_{eq}$ bond and one long Te–O$_{ax}$ bond and making angles of
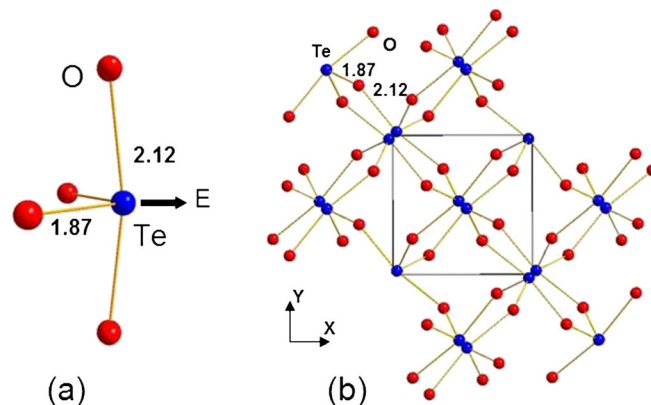
Figure 2. (a) Sketch of the disphenoidal unit TeO$_4$E (trigonal bipyramid; the arrow visualizes the direction of the lone pair E). (b) Projection in the Oxy plane of the structure of paratellurite.

741

$138.67°$. Remarkably, the isolated TeO_2 bent molecule with two Te O double bonds and with C_{2v} symmetry has a geometry very close to that of the $TeO_{2(eq)}$ grouping in α-TeO_2.[2,38] Hence, from a point of view of crystal chemistry, it can be considered that α-tellurite is a molecular crystal rather than a framework-like one. This point of view is strongly supported by valence force field calculations[39,40] and *ab initio* study of the vibrational properties of α-TeO_2.[41] Therefore, following this description, the vibrational modes of paratellurite can be classified into internal modes of the TeO_2 'molecules' and 'external modes' issued from the 'external' rotational and translational degrees of freedom of these entities. The internal modes comprise the symmetric combination of Te–O_{eq} stretching (v_1), the antisymmetric combination of Te–O_{eq} stretching (v_3), and the bending mode (v_2) of the O_{eq}–Te–O_{eq} angle. In the paratellurite unit cell that contains four such molecular units, these internal modes transform as

$$v_1 : A_1 + B_2 + E \qquad v_2 : A_1 + B_2 + E \qquad v_3 : A_2 + B_1 + E \quad (5)$$

However, the calculations[39–41] also show that if this description is fully valid for the v_1 and v_3 stretching modes occurring in the 500–$800\,cm^{-1}$ wavenumber range, no pure v_2 bending modes could be defined in the range 300–$400\,cm^{-1}$ where they are expected: In fact, the v_2 modes are strongly influenced by the Te–O_{ax} force constant and result in vibrations that rather characterize the Te–$_{eq}O_{ax}$–Te bridges.[39] Now, the so-called external modes include the optical modes corresponding to the translatory and rotatory (or librations) vibrations of the $TeO_{2(eq)}$ groups against each other, and they are expected in the low wavenumber range below ~$300\,cm^{-1}$.[39–41]

Results and discussion

In this study, for the RS and HRS measurements, we have used different right angle and backscattering geometries so as to set the momentum transfer vector **q** (i.e. the direction of propagation of the excited phonon modes) either parallel or perpendicular to the fourfold optical axis Oz. Under those conditions, we should be able to observe and to discriminate the pure TO and LO components of the polar modes with A_2 and E symmetries.[25,31,32] The results are summarized in Figs 3–6 and in Table 1. Note that we have adopted a logarithmic scale for the intensities of RS and HRS spectra to enhance the presence of low intensity but real signals.

Raman scattering

Figure 3 shows the Raman spectra obtained in a backscattering geometry where the directions of the incident and scattered lights are both set parallel to X', so that the momentum transfer vector **q** is set perpendicular to the Oz fourfold axis. The $X'(ZZ)\bar{X}'$ spectrum corresponds to the A_1 modes (α_{zz}), the $X'(Y'Y')\bar{X}'$ spectrum corresponds to the A_1 and B_2 modes ($\alpha_{y'y'}$), and the $X'(ZY')\bar{X}'$ spectrum corresponds to the E polar modes ($\alpha_{zy'}$). In the latter case, only the LO components are allowed.[15,31,32] Very clearly, these spectra do not show any significant polarization leakage. Three A_1 modes out of the four expected ones are observed at 148, 393, and $648\,cm^{-1}$ on the $X'(ZZ)\bar{X}'$ spectrum. According to the Section on Symmetry Properties of Paratellurite, the mode of the highest wavenumber at $648\,cm^{-1}$ is assigned to the A_1 component of the v_1 mode of the $TeO_{2(eq)}$ groups (Eqn (5)) and that at $393\,cm^{-1}$
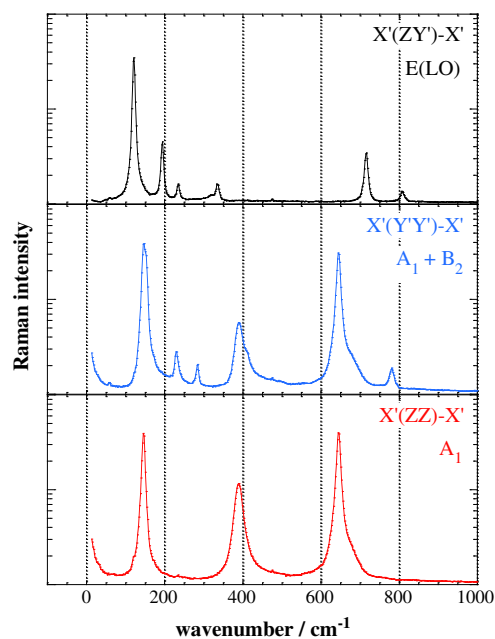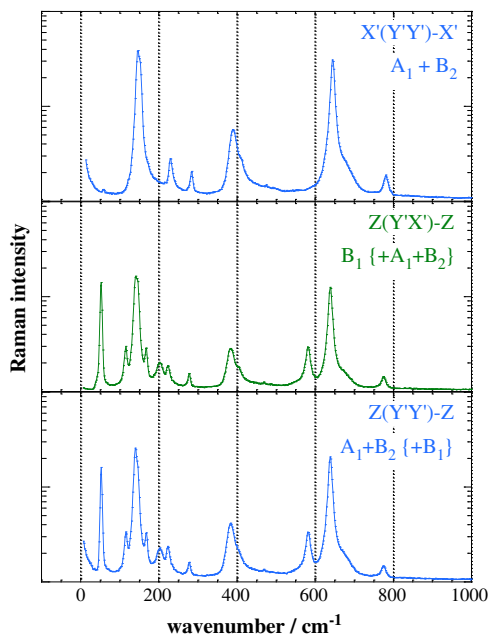
Figure 3. Polarized Raman spectra of paratellurite in the backscattering geometry. Raman intensity is in an arbitrary log scale.
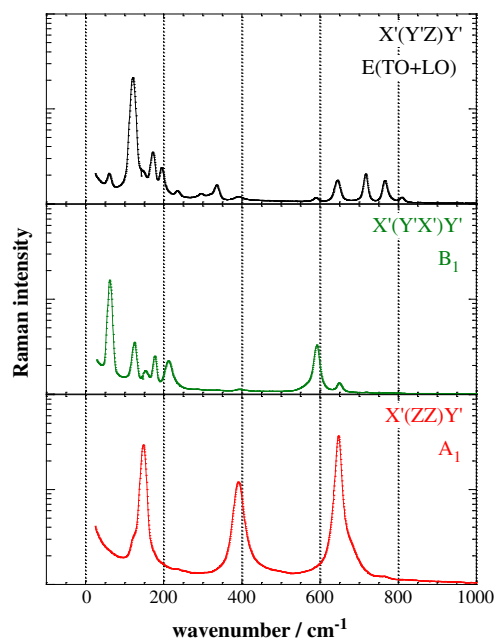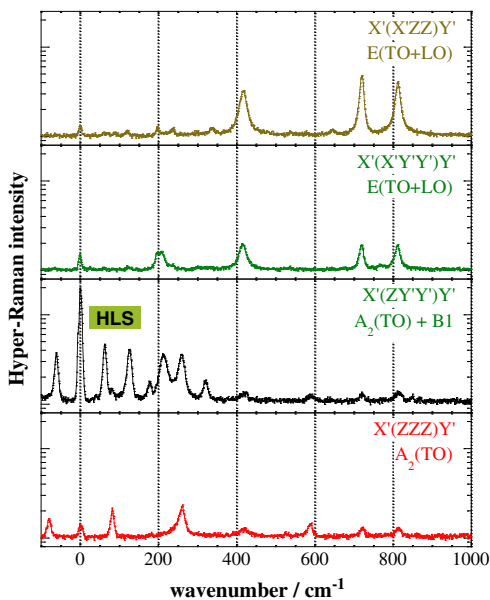
Figure 4. Polarized Raman spectra of paratellurite in the right angle geometry. Raman intensity is in an arbitrary log scale.

is assigned to a vibration of the Te–O–Te bridges issued from v_2. The remaining low wavenumber mode is then assigned to an external mode. On the $X'(Y'Y')\bar{X}'$ spectrum, in addition to the A_1 modes previously identified, four modes are clearly observed at 233, 287, 415, and $784\,cm^{-1}$ together with an additional unresolved shoulder at ~$150\,cm^{-1}$ on the high wavenumber side of the strong A_1 mode at $148\,cm^{-1}$. We note that the $233\,cm^{-1}$ line was already present as an extremely weak signal on the $X'(ZZ)\bar{X}'$ spectrum.

Figure 5. Polarized Raman spectra of paratellurite in the backscattering geometry. Raman intensity is in an arbitrary log scale. Note that both spectra (bottom) obtained with propagation of light along the main Z axis reveal a total loss of polarization information due to the strong optical rotation along the optical axis.

Figure 6. Polarized hyper-Raman spectra of paratellurite in the right angle geometry. Hyper-Raman intensity is in an arbitrary log scale. Note the harmonic light scattering (HLS) contribution in the $X'(ZY'Y')Y'$ geometry, which is Kleinman forbidden because it is an antisymmetric contribution.

So, in agreement with the *ab initio* calculations[41] and a previous Raman study,[15] we assign this line to the fourth expected A_1 mode corresponding to an external mode. Then, the four remaining lines at 150 (shoulder), 287, 415, and 784 cm^{-1} are assigned to the four expected B_2 modes. The mode of the highest wavenumber is assigned to the B_2 component of the v_1 mode of the TeO$_{2(eq)}$ groups (Eqn (5)), that at 415 cm^{-1} is assigned to a vibration of the O–Te–O bridges issued from v_2, and the two remaining low

Table 1. Summary of the lattice band assignments (wavenumbers in cm^{-1} ± 2 cm^{-1})

		A_1 (4/4)	A_2 (TO) (4/4)	B_2 (4/4)	B_1 (5/5)	E (TO) (8/8)	E (LO) (7/8)
Raman	$X'(ZZ)$-X': A_1	148, 393, 648	—	—	—	—	—
	$X'(ZY')$-X': E (LO)	—	—	—	—	—	122, 195, 235, 336, 717, 809
	$X'(Y'Y')$-X': $A_1 + B_2$	148, 233, 393, 648	—	150, 287, 415, 784	—	—	—
	$Z(Y'Y')$-Z: $A_1 + B_2$ {+B_1}	148, 233, 393, 648	—	150, 287, 415, 784	62, 125, 177, 210, 590	—	—
	$Z(Y'X')$-Z: B_1 {+$A_1 + B_2$}	148, 233 393, 648	—	150, 287, 415, 784	62, 125, 177, 210, 590	—	—
	$X'(ZZ)Y'$: A_1	148, 393, 648	—	—	—	—	—
	$X'(Y'Z)Y'$: E (TO+LO)	—	—	—	—	122, 173, 296, 392, 646, 767	—
	$X'(Y'X')Y'$: B_1	—	—	—	62, 125, 177, 212, 590	—	122, 196, 236, 337, 718, 811
	$X'(ZX)Y'$: E (TO+LO)	—	—	—	—	122, 173, 297, 336, 392, 645, 766	122, 195, 235, 718, 809
Hyper-Raman	$X'(ZZZ)Y'$: $A_2(Z)$ TO	—	82, 262, 592	—	—	Leaks of polarization	Leaks of polarization
	$X'(ZY'Y')Y'$: $A_2(Z)$ TO+B_1	HLS	82, 262, 321, 592	—	62, 125, 176, 212, 592	Leaks of polarization	Leak of polarization
	$X'(XZZ)Y'$: E (TO+LO)	—	—	—	—	122, 645	122, 197, 239, 337, 418, 720, 812
	$X'(X'Y'Y')Y'$: E (TO+LO)	—	—	—	—	122, 207, 764	122, 197, 239, 418, 720, 812

Figure 5 spectra labels:
$X'(Y'Y')$-X' — $A_1 + B_2$
$Z(Y'X')$-Z — B_1 {+A_1+B_2}
$Z(Y'Y')$-Z — A_1+B_2 {+B_1}

Figure 6 spectra labels:
$X'(X'ZZ)Y'$ — E(TO+LO)
$X'(X'Y'Y')Y'$ — E(TO+LO)
$X'(ZY'Y')Y'$ — A_2(TO) + B1 (HLS)
$X'(ZZZ)Y'$ — A_2(TO)

wavenumber modes are assigned to external vibrations. The $X'(ZY')\bar{X}'$ (Fig. 3) and $X'(Y'Z)\bar{X}'$ (not shown) spectra are identical and display six E (LO) modes (out of the eight expected ones) at 122, 195, 235, 336, 717, and 809 cm^{-1}. The two modes of highest wavenumber are assigned to the two expected E (LO) components of the v_1 and v_3 modes of the TeO$_{2(eq)}$ groups, the mode at 336 cm^{-1} is assigned to a mode of the Te–O–Te bridges issued from v_2, and the remaining three lines are assigned to external vibrations.

Figure 4 shows the Raman spectra obtained in a right angle scattering geometry where the direction of the incident light is set parallel to X' and that of the scattered light is set parallel to Y', so that the momentum transfer vector **q** is set perpendicular to the Oz fourfold axis as in the previous geometry. The $X'(ZZ)Y'$ spectrum corresponds to the A$_1$ modes (α_{zz}), the $X'(Y'X')Y'$ spectrum corresponds to the B$_1$ modes ($\alpha_{y'x'}$), and the $X'(ZY')Y'$ spectrum corresponds to the E polar modes ($\alpha_{y'z}$). In this configurations, both TO and LO components of the E modes are now allowed.[15,31,32] Again, the polarization leaks are very weak. As expected, the A$_1$ $X'(ZZ)Y'$ spectrum is identical to the $X'(ZZ)\bar{X}'$ spectrum previously described. The $X'(Y'X')Y'$ spectrum reveals the five expected B$_1$ modes, localized at 62, 125, 177, 210, and 590 cm^{-1}. This latter can be assigned to the B$_1$ component of the v_3 mode of the TeO$_{2(eq)}$ groups (Eqn (5)), and the other ones occurring at low wavenumber should be assigned to external vibrations. When comparing the $X'(Y'Z)Y'$ spectrum due to E (TO + LO) (Fig. 4) with the E (LO) spectrum shown in Fig. 3, we localize seven E (TO) modes (out of the eight expected ones) at 122, 173, 296, 336, 392, 646, and 767 cm^{-1}. Hence, the modes at 646 and 767 cm^{-1} are assigned to the E (TO) counterparts of the v_1 and v_3 E (LO) modes already observed at 717 and 809 cm^{-1} in backscattering geometry (Fig. 3).

Figure 5 shows the Raman spectra obtained in a backscattering geometry where the directions of the incident and of the scattered lights are both set parallel to the Z axis, so that the **q** vector is now directed parallel to the fourfold axis. The $Z(Y'X')\bar{Z}$ ($\equiv Z(X'Y')\bar{Z}$) spectrum is supposed to correspond to B$_1$ modes ($\alpha_{y'x'}$) (already shown in Fig. 4), and the $Z(Y'Y')\bar{Z}$ ($\equiv Z(X'X')\bar{Z}$) spectrum is supposed to correspond to the A$_1$ + B$_2$ modes ($\alpha_{y'y'}$) (already shown in Fig. 3 and reported also in Fig. 5 for comparison). In fact, the $Z(Y'X')\bar{Z}$ and $Z(Y'Y')\bar{Z}$ spectra are identical within the limit of experimental accuracy, because of quasi-perfect mixing of polarizations due to the strong optical activity of paratellurite acting on both the incident and scattered lights propagating along the fourfold axis, so resulting in a quasi-perfect mixing of the A$_1$ + B$_2$ ($\alpha_{y'y'}$) and B$_1$ ($\alpha_{x'y'}$) spectra.

To summarize our Raman data, all expected A$_1$, B$_1$, and B$_2$ modes have been clearly identified, and also, seven E (TO) and six E (LO) modes have been assigned out of the eight expected pairs of E modes (Table 1). Note also that the *ab initio* calculations[41] generally fit nicely with our interpretation of the Raman spectra, where is not for some differences in the peak positions.

Hyper-Raman scattering

To the best of our knowledge, we present in Fig. 6 the first study on HRS performed on paratellurite. As in previous Raman measurements, we have adopted a right angle scattering geometry where the direction of the incident light is set parallel to X' and that of the scattered light is set parallel to Y', so that the momentum transfer vector **q** is set perpendicular to the Oz

fourfold axis. Hence, the $X'(ZZZ)Y'$ spectrum corresponds to the A$_2$ (TO) polar modes (β_{zzz}), the $X'(ZY'Y')Y'$ spectrum corresponds to the A$_2$ (TO), and B$_1$ modes ($\beta_{zy'y'}$), and the $X'(X'Y'Y')Y'$ and X $(X'ZZ)Y'$ spectra both correspond to the E (TO + LO) modes ($\beta_{x'y'y'}$ and $\beta_{x'zz}$, respectively).[21,24,25] Three A$_2$ (TO) modes are clearly identified on the $X'(ZZZ)Y'$ spectrum at 82, 262, and 592 cm^{-1} (Fig. 6). All five B$_1$ modes already identified on the Raman spectra are observed on the $X'(ZY'Y')Y'$ spectrum, and the fourth expected A$_2$ (TO) mode is also identified at 321 cm^{-1} on this spectrum (Fig. 6). Following the arguments developed in the Section on Symmetry Properties of Paratellurite, the A$_2$ (TO) mode at 592 cm^{-1} is assigned to the expected A$_2$ component of the v_3 mode of the TeO$_{2(eq)}$ groups (Eqn (5)). The $X'(X'Y'Y')Y'$ and $X'(X'ZZ)Y'$ HRS spectra (Fig. 6) reveal most of the E (TO) and E (LO) modes already identified on the RS spectra and also exhibit two new lines at 207 and 418 cm^{-1} that cannot be seen on the RS spectra. According to published IR data,[15,16,18,19] the line at 207 cm^{-1} likely corresponds to a TO mode and that at 418 cm^{-1} corresponds to an LO mode.

To summarize our HRS data, all expected A$_2$ (TO) and B$_1$ modes have been detected, and all together, RS and HRS spectra exhibit the eight expected E (TO) modes and seven E (LO) modes (Table 1). In what concerns the polar A$_2$ and E modes, there is a good agreement between the wavenumbers determined by RS and HRS for the E modes, but we notice marked differences between our data and published IR data, which themselves do not always agree with each other. This can be explained by the fact that RS and HRS techniques provide us directly with the response functions of the TO and LO modes, whereas this information must be extracted from the IR reflectivity spectrum via a Kramers Kronig analysis (not used in the cited works) and/or by fitting the reflectivity data using phenomenological dielectric functions, where the wavenumbers and widths of the TO and LO modes are introduced as adjustable parameters. Note that additional hyper-Raman spectra have been performed at right angle geometry but with the fourfold axis in the plane of incidence (not shown). For both possible configurations, i.e. where the c axis is perpendicular to either the input side (case 1) or the output side (case 2), we observed also perfect mixing of polarization, as observed in RS (Fig. 5), owing to the strong optical rotation of light along the c axis at ω for case 1 and 2ω for case 2.

Harmonic light scattering

In the four hyper-Raman spectra reported in Fig. 6, we observe a weak or strong ($X'(ZY'Y')Y'$ spectrum) elastic contribution corresponding to harmonic light scattering. However, no HLS is expected under Kleinman condition because all the components of the symmetric part for the A$_1$ symmetry are zero.[21,24] A first possible origin of that extra contribution is connected to the second hyperpolarizability $\gamma(-2\omega; \omega,\omega, \Omega_{LO,TO})$ that generates an electro-optic (EO) contribution at the harmonic frequency under the effect of the LO or TO electric fields associated with the polar modes A$_2$ or E. Such EO contributions have already been observed in the case of HRS studies of cubic crystal NaCl.[23] In paratellurite, the EO effect is indeed expected in all HRS/HLS spectra because there are many nonzero components in the tetragonal D_4^4 structure.[21] However, we expect similar EO amplitude in the $X'(ZY'Y')Y'$ and $X'(X'ZZ)Y'$ spectra, which is not observed. A second possible origin of the strong HLS signal observed in the $X'(ZY'Y')Y'$ spectrum is connected to the

antisymmetric part of the A$_1$ species, which is out of the Kleinman condition, and supposed to be at the origin of the second harmonic generation signal observed by several authors.[11,12] For the D$_4$ point group, the HLS tensors for a biphotonic excitation in the Oxyz[27] and O$x'y'z$ frames are as follows:

$$A_1(Oxyz) : \begin{pmatrix} 0 & 0 & 0 & \lambda & 0 & 0 \\ 0 & 0 & 0 & 0 & -\lambda & 0 \\ 0 & 0 & 0 & 0 & 0 & \kappa \end{pmatrix} \quad (6)$$

$$\rightarrow A_1(Ox'y'z) : \begin{pmatrix} 0 & 0 & 0 & \lambda & 0 & 0 \\ 0 & 0 & 0 & 0 & -\lambda & 0 \\ \kappa & -\kappa & 0 & 0 & 0 & 0 \end{pmatrix}$$

If we consider the antisymmetric part of A$_1$ ($\lambda \neq 0$, $\kappa = 0$), which still corresponds to a pure dipolar electric term β^{eee}, we expect no HLS signal in the $X'(ZY'Y')Y'$ spectrum because $\beta_{ZY'Y'} = -\kappa = 0$ (Eqn (6)). In contrast, the mixed dipolar electric–magnetic term[42] β^{eem} of A$_1$ ($\lambda \neq 0$, $\kappa \neq 0$) gives an HLS signal in the $X'(ZY'Y')Y'$ spectrum because now $\beta_{ZY'Y'} = -\kappa \neq 0$. This dipolar electric–magnetic contribution at the microscopic level becomes at the macroscopic level the second harmonic generation optical rotation dispersion effect,[27,37] which is a nonlinear analog of the gyrotropic effect (linear optical rotation). As far as we know, this is indeed the first experimental evidence of hyper-Rayleigh scattering signal by an optically active material.

Conclusions

We investigated and revisited the Raman spectra of paratellurite. We showed that anomalous polarization-selection-rules violations previously observed and due to the optical activity are possible to avoid when light propagates at 45° of the Ox and Oy optical axes. Also, we presented for the first time an HRS study of paratellurite that complemented the IR and RS data. From this single crystal study, all expected optical phonon modes wavenumbers and symmetries are given, except one E (LO) mode that could not be observed. We have evidenced a strong harmonic light scattering signal in the $X'(ZY'Y')Y'$ spectrum that we tentatively assigned to hyper-Raleigh optical activity that comes from a mixed dipolar electric–magnetic effect.

References

[1] H. Beyer, *Z. Kristallogr.* **1967**, *124*, 228.
[2] P. A. Thomas, *J. Phys. C: Solid State Phys.* **1988**, *21*, 4611.
[3] T. G. Worlton, R. A. Beyerlein, *Phys. Rev. B.* **1975**, *12*, 1899.
[4] P. S. Peercy, I. J. Fritz, G. A. Samara, *J. Phys. Chem. Solids* **1975**, *36*, 1105.
[5] J. C. Champarnaud-Mesjard, S. Blanchandin, P. Thomas, A. P. Mirgorodsky, T. Merle-Méjean, B. Frit, *J. Phys. Chem. Solids* **2000**, *61*, 1499.
[6] S. Blanchandin, P. Marchet, P. Thomas, J. C. Champarnaud-Mesjard, B. A. Chagraoui, *J. Mat. Sci.* **1999**, *34*, 4285.
[7] J. F. Nye, *Physical Properties of Crystals*, Clarendon Press, Oxford, **1957**.
[8] G. Arlt, H. Schweppe, *Solid State Commun.* **1968**, *6*, 783.
[9] H. Schweppe, *Ultrasonics* **1970**, *8*, 84.
[10] N. Uchida, Y. Ohmachi, *Jpn. J. Appl. Phys.* **1970**, *9*, 155.
[11] D. S. Chemla, J. Jerphagnon, *Appl. Phys. Lett.* **1970**, *20*, 222.
[12] S. Singj, W. A. Bonner, L. G. Van Uitert, *Phys. Lett.* **1972**, *38A*(6), 407.
[13] C. Lasbrugnas, P. Thomas, O. Masson, J. C. Champarnaud-Mesjard, E. Fargin, V. Rodriguez, M. Lahaye, *Opt. Mater.* **2009**, *31*, 775.
[14] G. Guery, A. Fargues, T. Cardinal, M. Dussauze, F. Adamietz, V. Rodriguez, J. D. Musgraves, K. Richardson, P. Thomas, *Chem. Phys. Lett.* **2012**, *554*, 123.
[15] M. Krauzman, J. P. Mathieu, *C. R. Acad. Sci. Paris* **1971**, *273B*, 342.
[16] B. Ayrault, E. A. Descamps, F. Abba, Y. Marqueton, M. Durand, *Solid State Commun.* **1972**, *11*, 639.
[17] A. S. Pine, G. Dresselhaus, *Phys. Rev. B* **1972**, *5*, 4087.
[18] D. M. Korn, A. S. Pine, G. Dresselhaus, T. B. Reed, *Phys. Rev. B* **1973**, *8*, 768.
[19] N. N. Syrbu, R. V. Cretu, *Infrared Phys. Techn.* **1996**, *37*, 769.
[20] N. Mamedov, N. Yamamoto, Y. Shim, Y. Ninomiya, T. Takizawa, *Jpn. J. Appl. Phys. Part 1* **2003**, *42*, 5145.
[21] J. H. Christie, D. J. Lockwood, *J. Chem. Phys.* **1971**, *54*, 1141.
[22] V. Rodriguez, D. Talaga, F. Adamietz, J. L. Brunéel, M. Couzi, *Chem. Phys. Lett.* **2006**, *431*, 190.
[23] V. Rodriguez, *J. Raman Spectrosc.* **2012**, *43*, 627.
[24] S. J. Cyvin, J. E. Rauch, J. C. Decius, *J. Chem. Phys.* **1965**, *43*, 4083.
[25] V. N. Denisov, B. N. Mavrin, V. B. Podobedov, *Phys. Rep.* **1987**, *151*, 1.
[26] V. B. Podobedov, *J. Raman Spectrosc.* **1996**, *27*, 731.
[27] K. Verbiest, K. Clays, V. Rodriguez, *Second-Order Nonlinear Optical Characterizations Techniques: An Introduction*, CRC Press, New-York, **2009**.
[28] P. D. Maker, *Phys. Rev. A* **1970**, *1*, 923.
[29] P. Kaatz, D. P. Shelton, *Mol. Phys.* **1996**, *88*, 683.
[30] (a) O. Quinet, B. Champagne, V. Rodriguez, *J. Chem. Phys.* **2004**, *121*, 4705; (b) O. Quinet, B. Champagne, V. Rodriguez, *J. Chem. Phys.* **2006**, *124*, 244312.
[31] S. P. S. Porto, J. A. Giordmaine, T. C. Damen, *Phys. Rev.* **1966**, *147*, 608.
[32] R. Loudon, *Adv. Phys.* **1964**, *13*, 423.
[33] V. Kopsky, *Acta Cryst. A* **1979**, *35*, 83.
[34] N. Uchida, *Phys. Rev. B* **1971**, *4*, 3736.
[35] E. Yu Vorontsova, R. M. Grechishkin, I. A. Kaplunov, A. I. Kolesnikov, V. Ya Molchanov, S. A. Tret'yakov, *Opt. Spectrosc.* **2008**, *104*, 886.
[36] W. Kaminsky, E. Hartmann, *Z. Phys. B* **1993**, *90*, 47.
[37] V. Rodriguez, *J. Chem. Phys.* **2008**, *128*, 064707.
[38] D. W. Muenow, J. W. Hastie, R. Hauge, R. Bautista, J. L. Margrave, *Trans. Faraday Soc.* **1969**, *65*, 3210.
[39] A. P. Mirgorodsky, T. Merle-Méjean, J. C. Champarnaud-Mesjard, P. Thomas, B. Frit, *J. Phys. Chem. Solids* **2000**, *61*, 501.
[40] O. Noguera, PhD Thesis, University of Limoges, France **2003**. http://www.unilim.fr/scd.
[41] M. Ceriotti, F. Pietrucci, M. Bernasconi, *Phys. Rev. B* **2006**, *73*, 104304.
[42] D. L. Andrews, T. Thirunamachandran, *J. Chem. Phys.* **1979**, *70*, 1027.